Optogalvanic double-resonance spectroscopy in a neon discharge

K. Miyazaki,* H. Scheingraber, and C. R. Vidal
Institut für Extraterrestrische Physik Max-Planck-Institut für Physik und Astrophysik, D-8046 Garching bei München, Federal Republic of Germany
(Received 27 December 1982; revised manuscript received 9 June 1983)

A recently proposed method of optogalvanic double-resonance (OGDR) spectroscopy, which employs two cw lasers modulated at different frequencies and a dc discharge, has been investigated theoretically as well as experimentally. The technique is demonstrated to provide a versatile, state-selective spectroscopic method. A detailed analysis has been carried out for different situations where two lasers pump transitions which have the lower and/or upper state, or no state, in common. It also shows that the OGDR signal detected at the sum or difference modulation frequency can be given as a linear combination of the perturbed population densities in a plasma which give rise to the single-resonance signal. In addition, the results show that the OGDR signal polarity is characteristic for each type of double resonance. This has been verified in an OGDR experiment using a hollow-cathode discharge in neon and two cw dye lasers. State-selective OGDR spectra have been compared with optical-optical double-resonance spectra. Useful applications and advantages of the OGDR spectroscopy are discussed.

I. INTRODUCTION

Optogalvanic (OG) spectroscopy has been used extensively as a sensitive method for detecting atomic and molecular transitions in gas discharges and flames.[1] The convenient and versatile OG detection technique has been applied in various fields of spectroscopy such as Doppler-free spectroscopy,[2–8] two-photon and multiphoton spectroscopy,[7–10] two-step excitation spectroscopy,[11–14] level-crossing spectroscopy,[15] Penning-ionization spectroscopy,[16] plasma diagnostics,[17,18] atomic line-profile studies,[19] frequency locking of dye lasers,[20] and stabilization of gas lasers.[21,22]

The high sensitivity of the OG technique[23–25] results from the unique detection scheme which is based on a laser-induced impedance change in a plasma, and it allows one to observe weak absorption features between excited states of atomic or molecular species. However, the observed OG spectra are generally very dense,[26–28] and with respect to conventional emission and absorption spectra there is no significant advantage for the purposes of spectral assignments. On the other hand, despite several theoretical and experimental studies,[29–34] the detailed mechanism which is responsible for the OG effect appears to be not yet well understood. The lack of a detailed understanding of the OG effect itself has made it difficult to apply the OG technique to quantitative studies of atomic and molecular processes in plasmas.[35–37]

To facilitate the assignment of dense atomic and molecular spectra, optogalvanic double-resonance (OGDR) spectroscopy has recently been proposed by one of the present authors[38] as a new state-selective spectroscopic technique. The new method is widely applicable to transitions between excited atomic and/or molecular states generated in radiating plasmas, where most of the well-known state-selective methods such as laser-induced fluorescence[39] and laser-induced polarization spectroscopy[40] have a limited sensitivity due to the perturbing spontaneous emission. Furthermore, the OGDR spectroscopy has been suggested to allow quantitative studies of collisional energy transfer processes in a plasma.[38]

In this paper we report the first detailed theoretical and experimental study of the OGDR spectroscopy, and the new technique is demonstrated to provide a versatile state-selective spectroscopic method. The experimental arrangement considered consists of two tunable lasers modulated at different frequencies and a dc discharge. The OGDR signal induced by the two lasers is detected at the sum or difference modulation frequency with a lock-in amplifier. There have already been a few OG studies using two dye lasers which tried to make double-resonance experiments in a discharge.[11,12] These previous studies report the observation of OG signals originating from two-step one-photon excitation. The OGDR experiments described in this paper differ from those reported so far by detecting the double resonance at the sum or difference frequency of the modulation frequencies of two cw lasers.

The following section is devoted to the theory of the OGDR technique. We start with a basic analysis of the double-resonance experiment in order to clarify the origin of the OG signal at the sum or difference modulation frequency. For this purpose a rate-equation approach is used to describe the laser-induced population changes and the resulting OGDR signal in a plasma.

A general formalism is developed in a matrix notation, and the OGDR signal is shown to be directly related to a linear combination of the single-resonance signals. The general expressions are applied to the typical pumping schemes of double-resonance experiments indicated in Fig. 1. These four schemes are the most important ones for weakly ionized plasmas which are usually employed for OG experiments. In this paper the four pumping schemes indicated in Fig. 1 are denoted by N-, Λ-, V-, and P-type double resonance. The detailed analysis shows that the

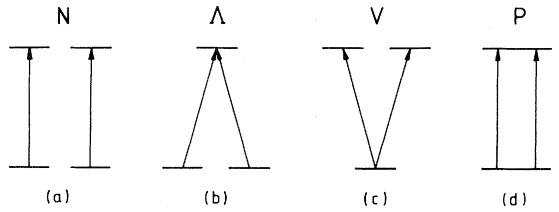

FIG. 1. Four types of double resonances, which are denoted by (a) N-, (b) Λ-, (c) V-, and (d) P-type double resonance in this paper.

polarity of the OGDR signal is characteristic to each type of double resonance and it predicts the typical properties of state-selective OGDR spectroscopy for different plasma conditions. For comparison, analytical expressions for the conventional optical-optical double-resonance (OODR) signal are also presented which in principle can provide similar informations to those given by the OGDR experiment.

Section III describes the OGDR experiment using a homemade hollow-cathode discharge in neon and two cw dye lasers, and the experimental results are presented in Sec. IV. In the experiment, special attention has been paid to the polarity of the OGDR signals to verify the theoretical predictions. Over a variety of experimental conditions, the OGDR signals are related to the single-resonance signals. For the V- and P-type double resonances the OGDR signals are shown to have a polarity opposite to those of the single-resonance signals, whereas for the N- and Λ-type double resonances the OGDR signals have a polarity identical with those of the single-resonance signals. These results agree with the theoretical predictions and allow the observation of state-selective OGDR spectra. State-selective OODR spectra have also been observed.

In Sec. IV we finally discuss the characteristic features and advantages of the OGDR spectroscopy, and further useful applications of this technique are suggested.

II. THEORETICAL

A. Basic equations

In the following we consider an experiment consisting of a dc discharge and two cw tunable lasers denoted by laser I and laser II. The laser beams propagate collinearly through the discharge plasma in the same or opposite directions, and the output frequency of each laser is tuned to some transition between excited levels of an atom or molecule in the plasma. We restrict our considerations to the small signal limit neglecting strong saturation phenomena due to laser-induced absorption. Furthermore, effects associated with the shape of the spectral lines will also be ignored which would have to be incorporated in an analysis of, for example, Doppler-free experiments.

By exposing the discharge to the radiation of the two lasers, the steady-state population density N_i^0 of some level $|i\rangle$ of an atom or molecule is changed by a small amount n_i and hence shifted to the new steady-state population density N_i. We may describe the population densities of all levels of interest in a compact notation by a vector

$$\vec{N}=\vec{N}^0+\vec{n}\ , \tag{1}$$

where the ith elements of the column vectors $\vec{N}$, $\vec{N}^0$, and $\vec{n}$ are the population densities N_i, N_i^0, and n_i, respectively, and we assume $|n_i| \ll N_i^0$. The change of the population densities $\vec{n}$ is, of course, a function of the absorption or pumping rates P_1, induced by laser I, and P_2, induced by laser II, which may be defined by

$$P_1=I_1\sigma_{ij},\quad P_2=I_2\sigma_{kl}\ , \tag{2}$$

respectively, where I_m is the intensity of laser M, and σ_{ij} is the absorption cross section for the transition between some lower level $|i\rangle$ and some upper level $|j\rangle$.

Let us assume that the intensities I_1 and I_2 are modulated periodically at the frequencies ω_1 and ω_2, respectively, e.g., by chopping the laser outputs, and that the resulting modulations of P_1 and P_2 are in the range of

$$0\le P_1\le 2P_{10},\quad 0\le P_2\le 2P_{20}\ , \tag{3}$$

corresponding to a range of the laser intensities of $0\le I_1\le 2I_{10}$ and $0\le I_2\le 2I_{20}$. As a result, the change of the population densities $\vec{n}$ and the population densities $\vec{N}$ become time-dependent functions of P_1 and P_2, $\vec{n}=\vec{n}(P_1,P_2)$ and $\vec{N}=\vec{N}(P_1,P_2)$.

The primary purpose of our analysis is to find the amplitude of the individual frequency components of $\vec{n}$ at ω_1,ω_2 and at the sum or difference frequencies $\omega_D=\omega_1\pm\omega_2$. If the modulated laser intensities do not vary faster than any one of the relaxation processes involved in the discharge, we have a quasistationary equilibrium of the plasma and the time-dependent change of $\vec{n}$ is governed only by the temporal histories of P_1 and P_2. Experimentally, this condition can be satisfied if ω_1 and ω_2 are sufficiently small, typically, less than a few kHz. In this case, the temporal change of $\vec{n}$ follows directly the temporal history of the laser intensities I_1 and I_2.

For the preceding conditions, the time-dependent frequency components of $\vec{n}$ may be found from a Taylor expansion of $\vec{n}(P_1,P_2)$. We expand $\vec{n}$ around $P_1=P_{10}$ and $P_2=P_{20}$ and obtain

$$\vec{n}=\vec{n}_0+\left[(P_1-P_{10})\left[\frac{\partial\vec{n}}{\partial P_1}\right]_0+(P_2-P_{20})\left[\frac{\partial\vec{n}}{\partial P_2}\right]_0\right]$$
$$+\frac{1}{2!}\left[(P_1-P_{10})^2\left[\frac{\partial^2\vec{n}}{\partial P_1^2}\right]_0+2(P_1-P_{10})(P_2-P_{20})\left[\frac{\partial^2\vec{n}}{\partial P_1\partial P_2}\right]_0+(P_2-P_{20})^2\left[\frac{\partial^2\vec{n}}{\partial P_2^2}\right]_0\right]+\cdots\ , \tag{4}$$

where the subscripts 0 indicate the quantities for $P_1=P_{10}$ and $P_2=P_{20}$. In Eq. (4), only the functions (P_1-P_{10}), (P_2-P_{20}) and their products depend on time and they describe the possible frequency components of $\vec{n}$ and their temporal histories. Therefore, the time-dependent population densities modulated at ω_1, ω_2, and ω_D are given directly by the second, third, and fifth term on the right of Eq. (4), neglecting small higher-order terms.[41] From Eq. (4), of course, one can also derive additional frequency components of $\vec{n}$ at $2\omega_1$, $2\omega_2$, $2\omega_1\pm\omega_2$, and so on. Within the range of P_1 and P_2 defined by Eq. (3), the corresponding terms of Eq. (4) lead to the amplitudes of the different frequency components of n_i, namely, n_i^{I} at ω_1 for $P_1=2P_{10}$, n_i^{II} at ω_2 for $P_2=2P_{20}$, and n_i^D at $\omega_D=\omega_1\pm\omega_2$ for $P_1=2P_{10}$ and $P_2=2P_{20}$ or $P_1=P_2=0$:

$$\vec{n}^{\,\mathrm{I}}=P_{10}(\partial\vec{n}/\partial P_1)_0 , \tag{5}$$

$$\vec{n}^{\,\mathrm{II}}=P_{20}(\partial\vec{n}/\partial P_2)_0 , \tag{6}$$

$$\vec{n}^{\,D}=\tfrac{1}{2}P_{10}P_{20}(\partial^2\vec{n}/\partial P_1\partial P_2)_0 , \tag{7}$$

where $\vec{n}^{\,\mathrm{I}}$, $\vec{n}^{\,\mathrm{II}}$, and $\vec{n}^{\,D}$ are vectors whose elements are n_i^{I}, n_i^{II}, and n_i^D, respectively.[42] It should be noted that only a steady-state value of $\vec{n}$ is necessary for obtaining further detailed expressions of Eqs. (5)—(7).

We consider a weakly ionized discharge such as a positive-column or a hollow-cathode discharge. The steady-state value of $\vec{n}$ may be calculated to a good approximation from a set of linearized rate equations for $\vec{N}$,[43,44]

$$d\vec{N}/dt=\underline{F}\vec{N}=0 , \tag{8}$$

where $\underline{F}$ is a matrix whose diagonal elements F_{ii} give the net depopulation rate of level $|i\rangle$ and whose off-diagonal elements F_{ij} give the population rate from level $|j\rangle$ to level $|i\rangle$. Substitution of Eq. (1) into Eq. (8) leads to

$$\underline{F}\cdot\vec{n}=\vec{P} . \tag{9}$$

In Eq. (9), $\vec{P}$ is the vector given by

$$\vec{P}=(\underline{F}^0-\underline{F})\cdot\vec{N}^{\,0} , \tag{10}$$

where $\underline{F}^0$ is the matrix $\underline{F}$ for $P_1=P_2=0$, and where we have used the steady-state rate equation, $\underline{F}^0\cdot\vec{N}^{\,0}=0$. Note that $\vec{P}$ is a constant vector containing only P_1, P_2, and $\vec{N}^{\,0}$ and is independent of any atomic processes in the discharge. The solution of Eq. (9) is straightforward, once an explicit expression for $\underline{F}$ is given.

Using Eq. (9), Eqs. (5) and (6) for $\vec{n}^{\,\mathrm{I}}$ and $\vec{n}^{\,\mathrm{II}}$ may be written in the form

$$\vec{n}^{\,M}=P_m(\underline{F}^{-1})_0\cdot\left[\frac{\partial\vec{P}}{\partial P_m}-\frac{\partial\underline{F}}{\partial P_m}\cdot\vec{n}_0\right] , \tag{11}$$

where $M=\mathrm{I}$ for $m=1$ and $M=\mathrm{II}$ for $m=2$. Since the elements of F and $\vec{P}$ are linear functions of P_1 and P_2, the derivatives in Eq. (11) are independent of P_1 and P_2, and consequently $\partial^2\underline{F}/\partial P_1\partial P_2=0$ and $\partial^2\vec{P}/\partial P_1\partial P_2=0$. The second derivative of Eq. (9), therefore, yields an alternative and convenient form for $\vec{n}^{\,D}$,

$$\begin{aligned}\vec{n}^{\,D}&=-\tfrac{1}{2}P_{10}P_{20}(\underline{F}^{-1})_0\cdot\left[\frac{\partial\underline{F}}{\partial P_1}\cdot\frac{\partial\vec{n}}{\partial P_2}+\frac{\partial\underline{F}}{\partial P_2}\cdot\frac{\partial\vec{n}}{\partial P_1}\right]_0\\&=-\tfrac{1}{2}P_{10}P_{20}(\underline{F}^{-1})_0\cdot\left[\frac{\partial\underline{F}}{\partial P_1}\cdot\left[\frac{\vec{n}^{\,\mathrm{II}}}{P_{20}}\right]+\frac{\partial\underline{F}}{\partial P_2}\cdot\left[\frac{\vec{n}^{\,\mathrm{I}}}{P_{10}}\right]\right] .\end{aligned} \tag{12}$$

Equation (12) is one of the key equations of this paper and shows that $\vec{n}^{\,D}$ is given as a linear combination of terms containing $\vec{n}^{\,\mathrm{I}}$ and $\vec{n}^{\,\mathrm{II}}$. In the following, we consider two different detection methods for $\vec{n}^{\,D}$.

(i) Optogalvanic detection. In general, the upper and lower levels of an atom or molecule which are perturbed by a laser, are closely coupled with other levels through radiative and collisional processes in the discharge. The overall change of the population densities causes a subsequent change of the electron density in the discharge plasma, giving rise to an impedance change of the discharge, i.e., the OG effect. This impedance change can be detected at $\omega_D=\omega_1\pm\omega_2$ as well as at ω_1 and ω_2, using the simple experimental arrangement shown in Fig. 2. The OG signals observed at ω_1, ω_2, and ω_D correspond to the detection of $\vec{n}^{\,\mathrm{I}}$, $\vec{n}^{\,\mathrm{II}}$, and $\vec{n}^{\,D}$, respectively, as shown below.

In the presence of two lasers, the electron density $N_e=N_e(P_1,P_2)$ in the discharge may be written in the form

$$N_e=N_e^0+n_e \tag{13}$$

analogous to Eq. (1), where N_e^0 is the unperturbed electron density, $n_e=n_e(P_1,P_2)$ is the laser-induced change of the electron density, and we assume again $|n_e|\ll N_e^0$. To a good approximation, n_e may be calculated from the steady-state rate equation for N_e,

$$dN_e/dt=(\vec{Q}\cdot\vec{N})N_e-\beta N_eN_{\mathrm{ion}}-\Gamma N_e=0 , \tag{14}$$

where N_{ion} is the ion density which is given by the charge-neutrality relation, $N_e\approx N_{\mathrm{ion}}$, in a plasma, $\vec{Q}$ is a vector whose element Q_i is the ionization coefficient of level $|i\rangle$ by electron impact, β is the radiative or two-body recombination coefficient for an electron and ion pair, and Γ denotes the diffusion loss rate of the electrons. Substituting Eqs. (1) and (13) into Eq. (14), we have

$$n_e=\beta^{-1}\vec{Q}\cdot\vec{n} . \tag{15}$$

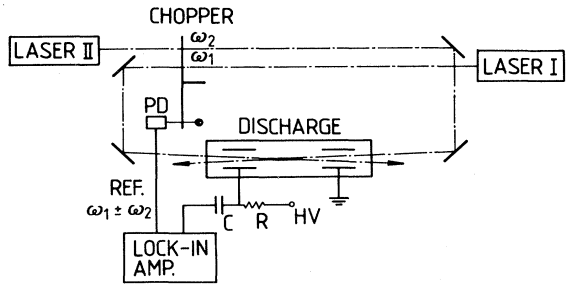

FIG. 2. Schematic arrangement of an OGDR experiment. PD, photodiode.

In the small signal limit of interest, one may assume that the impedance change or the OG signal S induced is proportional to the electron density change n_e, i.e., $S=\alpha n_e=\eta\vec{Q}\cdot\vec{n}$, where α is a proportionality constant, and $\eta=\alpha/\beta$. With the help of Eqs. (4)–(7), the OG signal amplitudes $S_{\rm I}$ observed at ω_1, $S_{\rm II}$ at ω_2, and S_D at ω_D are calculated as

$$S_{\rm I}=\eta\vec{Q}\cdot\vec{n}^{\,\rm I}\,, \tag{16}$$

$$S_{\rm II}=\eta\vec{Q}\cdot\vec{n}^{\,\rm II}\,, \tag{17}$$

$$S_D=\eta\vec{Q}\cdot\vec{n}^{\,D}\,. \tag{18}$$

It is important to note that $S_{\rm I}$, $S_{\rm II}$, and the OGDR signal S_D are given by linear functions of $\vec{n}^{\,\rm I}$, $\vec{n}^{\,\rm II}$, and $\vec{n}^{\,D}$, respectively. This linearity would still hold even if other possible mechanisms contributing to the OG signal, e.g., ionization by atom-atom collisions and so on, are incorporated in the rate equation for N_e.

(ii) Absorption measurement. Let us consider the conventional OODR experiment[44,45] in order to compare it with the OGDR technique. Figure 3 shows the principal arrangement of the experiment, in which only laser II (pump laser) is modulated at ω_2, whereas a fractional absorption of the unmodulated laser I (probe laser) is observed at ω_2 with a phase-sensitive detector. In this experiment, we redefine $P_1=P_{10}$, and the other experimental conditions are assumed to be identical with those in the OGDR experiment.

The decrease or increase ΔI_1 in the transmitted intensity I_1 of the modulated laser I can be calculated as

$$\begin{aligned}\Delta I_1&=\Delta x\,P_{10}(N_i-N_j)\\&=\Delta x\,P_{10}(N_i^0-N_j^0)+\Delta x\,P_{10}(n_i-n_j)\,,\end{aligned} \tag{19}$$

where the element Δx corresponds to a small absorption length. Following the procedure for obtaining Eqs. (5)–(7), we have the amplitude of the time-dependent ω_2 component of ΔI_1 or the resulting OODR signal S_0

$$\begin{aligned}S_0&=\zeta\,\Delta x\,P_{10}P_{20}\left[\frac{\partial(n_i-n_j)}{\partial P_2}\right]_0\\&=\zeta\,\Delta x\,P_{10}(n_i^{\rm II}-n_j^{\rm II})\,,\end{aligned} \tag{20}$$

where Eq. (6) has been used, and ζ is a proportionality constant depending on the sensitivity of the optical detector employed. In contrast to the OGDR signal S_D given by Eq. (18), Eq. (20) shows that S_0 results in a well-known manner only from the change of the population densities induced by laser II. A further detailed comparison of S_D and S_0 will be made in the subsequent sections.

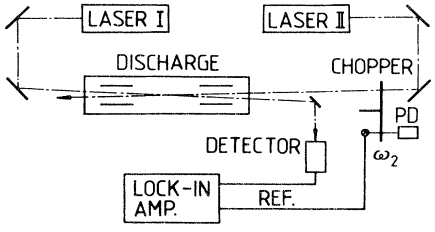

FIG. 3. Schematic arrangement of an OODR experiment. PD, photodiode.

B. Four-level system

In the following analyses, we apply the general expressions derived in the preceding section to the specific cases of the single- and double-resonance experiments. We consider a four-level system shown in Fig. 4, in which the lower levels are denoted by level $|1\rangle$ and level $|3\rangle$, and the upper levels by level $|2\rangle$ and level $|4\rangle$. For simplicity, these four levels are assumed to be nondegenerate, and the radiative and collisional processes indicated in Fig. 4 are taken into account as the dominant interaction processes among the four levels. The collisional excitation and deexcitation between the lower and upper levels may be ignored for a weakly ionized plasma of interest.

According to Fig. 4, a set of rate equations for N_i in the presence of two lasers can be written as

$$\begin{aligned}
dN_1/dt&=R_1-w_1-K_1N_1+A_{21}N_2+C_{31}N_3+A_{41}N_4=0\,,\\
dN_2/dt&=R_2-w_2-K_2N_2+C_{42}N_4=0\,,\\
dN_3/dt&=R_3-w_3-K_3N_3+C_{13}N_1+A_{23}N_2+A_{43}N_4=0\,,\\
dN_4/dt&=R_4-w_4-K_4N_4+C_{24}N_2=0\,,
\end{aligned} \tag{21}$$

where A_{ji} is the effective transition probability due to radiation from level $|j\rangle$ to level $|i\rangle$, $C_{ij}N_i$ denotes the collisional population rate from level $|i\rangle$ to level $|j\rangle$, w_i is the population or depopulation rate of level $|i\rangle$ due to the laser pumping, R_i is the net population rate of level $|i\rangle$ due to the remaining processes, and K_iN_i is the net depopulation rate of level $|i\rangle$ due to atomic processes in the plasma.

The rate w_i is a linear function of $N_i=N_i^0+n_i$. Hence, substituting Eq. (1) into Eq. (21) and setting

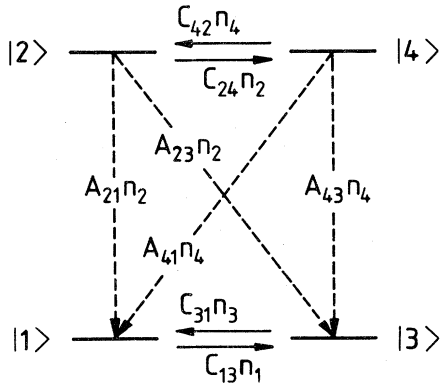

FIG. 4. Four-level system employed for the analysis of the double-resonance experiments. Radiative and collisional interaction processes among the four levels are indicated by the dashed and solid arrows, respectively, together with the population rates.

$$\underline{F}=\underline{F}^0+\underline{W}\ , \tag{22}$$

$$\vec{P}=-\underline{W}\vec{N}^0\ , \tag{23}$$

we have the rate equation for $\vec{n}$ in the form of Eq. (9), where the ith element of the column vector $\vec{w}=\underline{W}(\vec{N}^0+\vec{n}),=\underline{W}\vec{N}$ is w_i, and

$$\underline{F}^0=\begin{vmatrix} -K_1 & A_{21} & C_{31} & A_{41} \\ 0 & -K_2 & 0 & C_{42} \\ C_{13} & A_{23} & -K_3 & A_{43} \\ 0 & C_{24} & 0 & -K_4 \end{vmatrix}\ . \tag{24}$$

C. Single resonance

We start with an OG experiment using only a single laser beam (laser I) which is tuned to the resonance transition $|1\rangle-|2\rangle$, i.e., $P_1=I_1\sigma_{12}$. Substituting $w_1=-w_2=P_1(N_1-N_2)$ and $w_3=w_4=0$ into Eq. (21), one obtains the rate equation for $\vec{n}=(n_1,n_2,n_3,n_4)$ in the form of Eq. (9). The matrix $\underline{F}$ and the vector $\vec{P}$ are given by Eqs. (22) and (23) with

$$\underline{W}=P_1\underline{D}(1,2) \tag{25}$$

where the elements of the matrix $\underline{D}(a,b)$ are given by

$$D_{ik}(a,b)=(\delta_{ib}-\delta_{ia})(\delta_{ka}-\delta_{kb}) \tag{26}$$

with δ_{mn} being the Kronecker symbol.

In order to express the solution $\vec{n}=\underline{F}^{-1}\vec{P}$ and the resulting quantities of interest in a concise manner, without loosing the physical significance we define the transition probabilities

$$\gamma_{ji}=A_{ji}+C_{jl}(A_{li}\tau_l)\ , \tag{27}$$

$$\xi_{ji}=A_{ji}+A_{jk}(C_{ki}\tau_k)\ , \tag{28}$$

where $\tau_i=K_i^{-1}$ is the effective lifetime of level $|i\rangle$ in the discharge plasma of interest. The quantities defined by Eqs. (27) and (28) can be regarded as the effective transition probabilities from the upper level $|j\rangle$ to the lower level $|i\rangle$ due to the following radiative (rad) and collisional (coll) processes for γ_{ji} and ξ_{ji}, respectively:

$$|j\rangle\xrightarrow{\text{rad}}|i\rangle+|j\rangle\xrightarrow{\text{coll}}|l\rangle\xrightarrow{\text{rad}}|i\rangle\ ,$$

$$|j\rangle\xrightarrow{\text{rad}}|i\rangle+|j\rangle\xrightarrow{\text{rad}}|k\rangle\xrightarrow{\text{coll}}|i\rangle\ .$$

Then, $\underline{F}^{-1}$ can be given in the form

$$\underline{F}^{-1}=\underline{H}/F_1(1,2)\ , \tag{29}$$

where

$$\underline{H}=\begin{vmatrix} -\tau_1u_{24} & -\tau_1(\Phi_{21}\tau_2) & -\tau_1(C_{31}\tau_3)u_{24} & -\tau_1(\Phi_{41}\tau_4) \\ 0 & -\tau_2u_{13} & 0 & -\tau_2(C_{42}\tau_4)u_{13} \\ -\tau_3(C_{13}\tau_1)u_{24} & -\tau_3(\Phi_{23}\tau_2) & -\tau_3u_{24} & -\tau_3(\Phi_{43}\tau_4) \\ 0 & -\tau_4(C_{24}\tau_2)u_{13} & 0 & -\tau_4u_{13} \end{vmatrix}\ , \tag{30}$$

with

$$\Phi_{ji}=\gamma_{ji}+\gamma_{jk}(C_{ki}\tau_k)=\xi_{ji}+C_{jl}(\xi_{li}\tau_i)\ , \tag{31}$$

$$u_{ik}=u_{ki}=1-(C_{ik}\tau_i)(C_{ki}\tau_k)\ , \tag{32}$$

and

$$F_m(i,j)=(\det\underline{F})^m(u_{13}u_{24})^{-m+1}$$
$$\approx u_{13}u_{24}+mP_1[\tau_i(u_{24}-\Phi_{ji}\tau_j)+\tau_ju_{13}]\ . \tag{33}$$

In Eq. (30), small higher-order corrections to the matrix elements H_{ij} of $\underline{H}$ have been ignored. Using Eq. (11) and the solution for $\vec{n}$, $\vec{n}^{\,I}$ is obtained as

$$\vec{n}^{\,I}=(N_1^0-N_2^0)P_{10}\vec{B}(1,2)/[F_2(1,2)]_0\ . \tag{34}$$

Here, the kth element $B_k(i,j)$ of the column vector $\vec{B}(i,j)$ is given by

$$B_k(i,j)=H_{ki}-H_{kj}\ , \tag{35}$$

to the lowest order considered. With the substitution of Eq. (34) into Eq. (16), the OG signal S_I at ω_1 is given by

$$S_I=\eta P_{10}(N_1^0-N_2^0)G(1,2)/[F_2(1,2)]_0\ , \tag{36}$$

where

$$G(i,j)=\vec{Q}\cdot\vec{B}(i,j)=\sum_k Q_k(H_{ki}-H_{kj})=-G(j,i)\ . \tag{37}$$

The function $G(i,j)$ defined by Eq. (37) may be called the "OG function" and it depends only on the specific discharge conditions. This function is responsible for the sign of S_I, because $[F_2(1,2)]_0$ and $(N_1^0-N_2^0)$ in Eq. (36) are positive under typical discharge conditions. Note that the OG function is characteristic for the OG detection and may be regarded as a conversion factor for the laser-induced absorption, $P_{10}(N_1^0-N_2^0)$, into the OG signal. When neither radiative nor collisional interactions shown in Fig. 4 are of importance in the discharge, Eq. (36) reduces to the form given by Erez *et al.*[31] It should be mentioned that the rate-equation approach employed is valid under the condition, $P_1\tau_i\ll 1$, in Eq. (33), which corresponds to the experiment in the small signal limit.[45]

D. Double resonance

Based on the analysis for the single-resonance experiment, we consider the OGDR experiment using both lasers I and II. Laser I and laser II are assumed to be on resonance with the transitions $|i\rangle-|j\rangle$ and $|k\rangle-|l\rangle$, respectively, i.e., $P_1=I_1\sigma_{ij}$ and $P_2=I_2\sigma_{kl}$. The following derivation of the four different types of double resonances shown in Fig. 1 is carried out by assigning the states $|1\rangle$, $|2\rangle$, $|3\rangle$, and $|4\rangle$ of Fig. 4 to the indices i, j, k, and l ac-

cording to Table I. In this manner all the subsequent results apply to any one of the four different types of double resonances using the appropriate indices.

The rate equations for N_i are given by Eq. (21). Similar to the preceding section the rate equations for n_i are given by Eqs. (9) and (22) with

$$\overline{W}=P_1\underline{D}(i,j)+P_2\underline{D}(k,l)\ , \tag{38}$$

where the D matrices are defined in Eq. (26).

The matrices $\underline{F}$ and $\vec{P}$ can be readily calculated, and lead to the general form for the perturbed population density $\vec{n}$,

TABLE I. Assignment of the states $|1\rangle$, $|2\rangle$, $|3\rangle$, and $|4\rangle$ to the indices i, j, k, and l for the four different types of double resonances.

	i	j	k	l
N	1	2	3	4
Λ	1	2	3	2
Λ	1	4	3	4
V	1	2	1	4
V	3	2	3	4
P	1	2	1	2
P	3	4	3	4

$$\vec{n}=[(N_i^0-N_j^0)P_1\vec{B}(i,j)+(N_k^0-N_l^0)P_2\vec{B}(k,l)]/\underline{F}_l(i,j;k,l)\ , \tag{39}$$

where

$$\begin{aligned}F_m(i,j;k,l)&=(\det\underline{F})^m(u_{13}u_{24})^{-m+1}\\&\approx u_{13}u_{24}+mP_1[\tau_i(u_{24}-\Phi_{ji}\tau_j)+\tau_j u_{13}]+mP_2[\tau_k(u_{24}-\Phi_{lk}\tau_l)+\tau_l u_{13}]\ ,\end{aligned} \tag{40}$$

and where we have used $\underline{F}^{-1}=\underline{H}/\underline{F}_l(i,j;k,l)$. Using Eqs. (11) and (12), one obtains the ω_1, ω_2, and ω_D components of $\vec{n}$,

$$\vec{n}^{\,\mathrm{I}}=(N_i^0-N_j^0)P_{10}\vec{B}(i,j)/[F_2(i,j;k,l)]_0\ , \tag{41}$$

$$\vec{n}^{\,\mathrm{II}}=(N_k^0-N_l^0)P_{20}\vec{B}(kl)/[F_2(i,j;k,l)]_0\ , \tag{42}$$

$$\vec{n}^{\,D}=\tfrac{1}{2}[(n_i^{\mathrm{II}}-n_j^{\mathrm{II}})P_{10}\vec{B}(i,j)+(n_k^{\mathrm{I}}-n_l^{\mathrm{I}})P_{20}\vec{B}(k,l)]/[\underline{F}_l(i,j;k,l)]_0\ . \tag{43}$$

Note that $\vec{n}^{\,D}$ is given by two terms in a form similar to those of Eqs. (41) and (42). Each term contains a product of the pump rate due to laser I and the population densities perturbed by laser II, and vice versa. This allows one to interpret $\vec{n}^{\,D}$ as a second-order population change by the following two-step processes: lasers I and II induce $\vec{n}^{\,\mathrm{I}}$ and $\vec{n}^{\,\mathrm{II}}$ at ω_1 and ω_2, respectively, and the subsequent pumping processes of $\vec{n}^{\,\mathrm{II}}$ by laser I and of $\vec{n}^{\,\mathrm{I}}$ by laser II generate $\vec{n}^{\,D}$ at ω_D.

Substituting Eqs. (41) and (42) into Eq. (43), we have an alternative expression for $\vec{n}^{\,D}$,

$$\vec{n}^{\,D}=\tfrac{1}{2}P_{10}P_{20}[(N_i^0-N_j^0)h(k,l;i,j)\vec{B}(k,l)+(N_k^0-N_l^0)h(i,j;k,l)\vec{B}(i,j)]\{u_{13}u_{24}[F_3(i,j;k,l)]_0\}^{-1}\ , \tag{44}$$

where $h(i,j;k,l)$ is given by the elements of $\vec{B}(k,l)$ or by the matrix elements of $\underline{H}$ as

$$\begin{aligned}h(i,j;k,l)&=B_i(k,l)-B_j(k,l)=H_{ik}-H_{il}-(H_{jk}-H_{jl})\\&=h(j,i;l,k)=-h(j,i;k,l)=-h(i,j;l,k)\ .\end{aligned} \tag{45}$$

The sign of $h(i,j;k,l)$ depends only on the plasma conditions.

Substituting the results for $\vec{n}^{\,\mathrm{I}}$, $\vec{n}^{\,\mathrm{II}}$, and $\vec{n}^{\,D}$ into Eqs. (16)—(18), we have the OG signals S_{I} at ω_1, S_{II} at ω_2, and S_D at ω_D,

$$S_{\mathrm{I}}=\eta P_{10}(N_i^0-N_j^0)G(i,j)/[F_2(i,j;k,l)]_0\ , \tag{46}$$

$$S_{\mathrm{II}}=\eta P_{20}(N_k^0-N_l^0)G(k,l)/[F_2(i,j;k,l)]_0\ , \tag{47}$$

$$S_D=\tfrac{1}{2}\eta[(n_i^{\mathrm{II}}-n_j^{\mathrm{II}})P_{10}G(i,j)+(n_k^{\mathrm{I}}-n_l^{\mathrm{I}})P_{20}G(k,l)]/[\underline{F}_l(i,j;k,l)]_0 \tag{48}$$

$$=\tfrac{1}{2}\eta P_{10}P_{20}[(N_i^0-N_j^0)h(k,l;i,j)G(k,l)+(N_k^0-N_l^0)h(i,j;k,l)G(i,j)]\{u_{13}u_{24}[F_3(i,j;k,l)]_0\}^{-1}\ . \tag{49}$$

Comparison of Eq. (41) with Eq. (34) or of Eq. (46) with Eq. (36) reveals a slight difference arising from the denominators. This implies that in the double-resonance experiment, laser II modulated at ω_2 exerts an effect on the ω_1 component $\vec{n}^{\,\mathrm{I}}$ and decreases the resulting OG signal S_{I}. In fact, this effect was observed in the OGDR experiment described in Sec. III.

Equations (48) and (49) show that S_D is given by a linear superposition of two OG functions, each of which is the same as that in Eqs. (46) and (47). The sign or polarity of S_D is found to depend only on the atomic processes in the discharge concerned, although the polarity cannot always be predicted without a detailed knowledge of the rate coefficients. However, under the following conditions of a discharge we can discuss the definite polarity of S_D for the four types of double resonances of interest and the possibility of state-selective spectroscopy by means of the OGDR experiment.

Since only the OG functions $G(i,j)$ and $G(k,l)$ are responsible for the polarities of $S_{\rm I}$ and $S_{\rm II}$, we are able to determine experimentally the sign of the two OG functions from independent observations of $S_{\rm I}$ and $S_{\rm II}$. Hence by controlling the discharge conditions such as discharge current and gas pressure, it is possible to find discharge conditions which provide $S_{\rm I}S_{\rm II}>0$ or $G(i,j)G(k,l)>0$. Then, S_D is expected to have a definite polarity for the following plasma conditions which are often encountered in OG experiments and may be generated, for example, using a positive column, hollow-cathode discharge or other discharges.

(a) The first example is a plasma in which radiative processes are dominant for the relaxation of the perturbed population densities, and collisional interactions can be ignored. For the four types of double resonances, the simplified form of S_D calculated from Eq. (49) is given and discussed in the Appendix. The corresponding polarity of S_D is summarized in Table II together with those for the other cases (b) and (c) considered below. Note that S_D for the V- and P-type double resonances has a polarity opposite to that of $S_{\rm I}$ and $S_{\rm II}$, whereas S_D for the N- and Λ-type double resonances has an identical polarity with that of $S_{\rm I}$ and $S_{\rm II}$. Let us assume an OGDR experiment in which one of the two tunable lasers is scanned over a given spectral range, whereas the other is pumping a specific transition in the discharge. The polarity relation of S_D for the four different types of double resonances suggests that one can immediately discern the transitions with a common lower level. It is clear that transitions pertaining to different atomic and molecular species in the discharge give no signal in the OGDR spectrum. Such a state-selective OGDR spectrum may be observed in a weakly ionized discharge which is usually employed for OG experiments where radiative processes dominate the relaxation of the excited levels perturbed.

(b) The second example is a plasma in which both collisional and radiative interactions shown in Fig. 4 can be ignored for the relaxation of the relevant excited levels, i.e., $\Phi_{ji}\tau_j$, $C_{jl}\tau_j\approx 0$. In this case, the N-type double resonance is found to be unobservable from Eq. (49), and the polarity of S_D derived for the other types of double resonances is given in Table II. In an OGDR spectrum, the Λ-, V-, and P-type double resonances map out the transitions which share the lower and/or upper level with the pump transition. In this case Eq. (45) for the Λ-type double resonance reduces to $-\tau_2$ and for the V- and P-type double resonances one obtains $-\tau_1$ and $-(\tau_1+\tau_2)$, respectively. For a situation $\tau_2\ll\tau_1$, which is usually expected in a weakly ionized discharge, the OGDR signal S_D due to a Λ-type double resonance will become fairly small compared with the signal originating from the V- and P-type double resonances. In such a case, one observes only transitions with a common lower level in an OGDR spectrum. This type of state selectivity in the OGDR spectrum may be realized in a molecular plasma, where in general radiative cascade processes to a specific level are unimportant due to the small transition probabilities, and where collisional interactions can be suppressed in a low-pressure and low-current discharge.

(c) If collisions play a dominant role in the plasma of interest, S_D is found to have an identical polarity for all the four types of double resonances, as shown in Table II. In this case, the OGDR technique appears to be of little use for the purposes of simplifying OG spectra. However, the collisional interactions in a plasma can be very selective. In addition, the OGDR signals due to collision-induced transitions are expected to be much smaller than those due to the V- and P-type double resonances. Therefore, under favorable conditions, the OGDR spectrum in a collision-dominated plasma would still be very simple.

OGDR experiments under any one of the preceding discharge conditions allow one to perform state-selective spectroscopy of atoms and molecules. The OGDR spectra observed are easy to identify and greatly facilitate the assignment of individual atomic or molecular transitions.

From Eq. (20), we obtain the OODR signal S_0 for the four different types of double resonances. The general form of S_0 is

$$S_0=\xi\,\Delta x\,P_{10}(n_i^{\rm II}-n_j^{\rm II})$$
$$=\xi\,\Delta x\,P_{10}P_{20}(N_k^0-N_l^0)h(i,j;k,l)/[F_2(i,j;k,l)]_0\ . \tag{50}$$

Equations (48) or (49) and (50) show that both OGDR and OODR experiments measure a modulated population density $\vec{n}$ of the same order. The polarity of S_0 is governed by the function $h(i,j;k,l)$ in Eq. (50). For the three typical plasma conditions discussed above, and for the four types of double resonances S_0 is found to have the same

TABLE II. Polarities of the OGDR signal in a plasma where (a) radiative processes, (b) no collisional and radiative interactions, and (c) collisional processes are dominant for the relaxation of the perturbed population densities.

		S_D			
	$S_{\rm I},S_{\rm II}$	N	Λ	V	P
(a)	+	+	+	−	−
	(−)	(−)	(−)	(+)	(+)
(b)	+		−	−	−
	(−)		(+)	(+)	(+)
(c)	+	−	−	−	−
	(−)	(+)	(+)	(+)	(+)

polarity relation as that for S_D shown in Table II. In the OODR experiment, the restricted discharge condition of $S_I S_{II} > 0$, of course, is not necessary for state-selective spectroscopy.

III. EXPERIMENT

To demonstrate the OGDR technique, an experiment was carried out using a homemade hollow-cathode discharge and two commercial cw dye lasers, a ring dye laser pumped by a krypton ion laser, and a linear dye laser pumped by an argon ion laser. We have employed a discharge in pure neon for the experiment because neon has a very simple system of energy levels and convenient transitions for the observation of the four different types of double resonances. Table III summarizes the excited neon levels (in Paschen notation) of interest and the allowed transitions together with the gf values characterizing the transition moments.[46]

When the transitions between the $1s$ and $2p$ levels in a weakly ionized neon discharge are pumped by the two lasers, the relaxation of the modulated population densities of the upper $2p$ levels will be dominated by radiative processes to the lower $1s$ levels. Then, the OGDR signals observed for the four types of double resonances are expected to have the polarity of case (a) discussed above and summarized in Table II. The theoretical prediction on the polarity of S_D has been tested over a variety of experimental conditions. Furthermore, the state-selective OGDR spectra which are also predicted in the preceding section have been observed together with OODR spectra. In this section, we describe the experimental procedure, and the results obtained are presented in Sec. IV.

A. Experimental arrangement

The experimental arrangement employed is shown schematically in Fig. 5. The ring and linear dye lasers are both operated with Rhodamine-6G in the spectral range of 565—634 nm. They have identical linear polarizations and have typical spectral widths of 3 and 30 GHz, respectively. The beams of the ring and linear dye lasers are modulated by a mechanical chopper at different frequencies $\omega_1 = 550$ Hz and $\omega_2 = 825$ Hz. The two beams are sent through the discharge tube in opposite directions forming a small angle between each other to avoid optical feedback between the different dye-laser cavities.

The discharge tube with Brewster-angle windows has a coaxial structure consisting of a hollow cathode of 5 mm in bore diamter and 40 mm in effective discharge length and two anodes of 5 mm in bore diameter. The three electrodes are made of copper and are cooled with flowing water. The neon gas is continuously pumped at a constant flow rate, and the pressure was varied over a range of 0.05—10 Torr. The discharge current was varied over a range of 2—18 mA, corresponding to an applied dc voltage of 0.5—2.6 kV. Under these discharge conditions, a very stable plasma was generated with an overall discharge noise of typically a few mV as observed on a cathode-ray oscilloscope (CRO).

The discharge circuit contains large ballast resistors (R) to maintain a constant current and to convert the laser-

TABLE III. Energy levels and wavelength (nm) for the transitions $1s_i$-$2p_j$. gf values are also given in parentheses.

Level	(cm^{-1})	$2p_{10}(^3S_1)$ 148 260	$2p_9(^3D_3)$ 149 659	$2p_8(^3D_2)$ 149 826	$2p_7(^3D_1)$ 150 124	$2p_6(^1D_2)$ 150 318	$2p_5(^1P_1)$ 150 774	$2p_4(^3P_2)$ 150 860	$2p_3(^3P_0)$ 150 919	$2p_2(^3P_1)$ 151 040	$2p_1(^1S_0)$ 152 973
$1s_5(^3P_2)$	134 044	703.2	640.2	633.4	621.7	614.3	597.6	594.5		588.2	
		(0.563)	(2.211)	(0.484)	(0.111)	(0.798)	(0.0564)	(0.299)		(0.179)	
$1s_4(^3P_1)$	134 461	724.5		650.7	638.3	630.5	612.8	609.6	607.4	603.0	540.1
		(0.221)		(0.952)	(0.588)	(0.124)	(0.011)	(0.504)	(0.334)	(0.0917)	(0.0039)
$1s_3(^3P_0)$	134 821	743.9			653.3		626.7			616.4	
		(0.0575)			(0.207)		(0.440)			(0.249)	
$1s_2(^1P_1)$	135 891	808.2		717.4	702.4	692.9	671.7	667.8	665.2	659.9	585.2
		(0.0035)		(0.111)	(0.0419)	(0.626)	(0.440)	(0.779)	(0.0019)	(0.454)	(0.350)

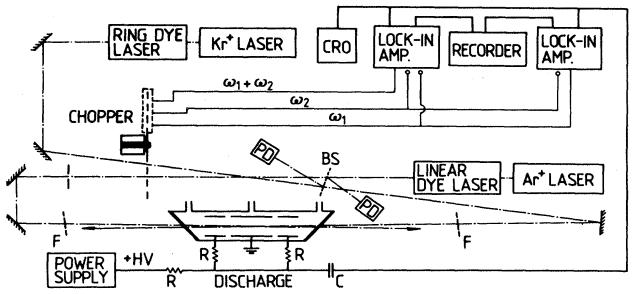

FIG. 5. Schematic diagram of the arrangement employed for the OGDR experiment. PD, photodiodes; BS, beam splitter; CRO, oscilloscope; F, neutral-density filters.

induced impedance change into a voltage change. The OG signal is extracted by a capacitor (C), and the modulated signal is observed on an oscilloscope. The OGDR signal is detected at the sum frequency, $\omega_D = 1375$ Hz, with a lock-in amplifier and is measured on a strip chart recorder. Another lock-in amplifier is employed to monitor the OG signal at ω_1 or ω_2. Owing to the polarity of the high voltage applied to the discharge, the electric circuit employed provides a negative OG signal for an increase of electron density in the discharge and vice versa. This means that the proportionality constant η defined in Sec. II is negative in the present experiment.

B. Signal polarity

In the following, the ring dye laser and the linear dye laser are denoted by laser I and laser II, respectively. For demonstrating the theoretical predictions, it is crucial to know the polarities of $S_{\rm I}$, $S_{\rm II}$, and S_D. The polarities of $S_{\rm I}$ and $S_{\rm II}$ can be easily determined on an oscilloscope by independent direct observations of the modulated OG signals at ω_1 and ω_2, respectively. However, it is clear that such a direct observation of the polarity of S_D is difficult. In the presence of lasers I and II, the superimposed OG signal observed on an oscilloscope is simply the sum of two modulated single-resonance signals, which is certainly not the OGDR signal of interest. Therefore, the following procedure was employed to determine the polarity of S_D.

Let $\phi_{\rm I}$, $\phi_{\rm II}$, and ϕ_D be the phase angle of the lock-in amplifier associated with $S_{\rm I}$, $S_{\rm II}$, and S_D, respectively. As discussed in Sec. II, the temporal histories of the OG signals at ω_1, ω_2, and ω_D follow the time-dependent modulated wave form of (P_1-P_{10}), (P_2-P_{20}), and $(P_1-P_{10})(P_2-P_{20})$, respectively. Then, one may expect the simple relationship

$$\phi_D \approx \phi_{\rm I} + \phi_{\rm II}(\pm 360^\circ) . \tag{51}$$

When a maximum amplitude of the OGDR signal is observed at a phase angle ϕ with the lock-in amplifier, ϕ should be $\phi \approx \phi_D$ or $\phi \approx \phi_D \pm 180^\circ$. Since $\phi_{\rm I}$ and $\phi_{\rm II}$ can be easily measured, the correct phase angle or resulting polarity of S_D can be determined with the help of Eq. (51). The relation given by Eq. (51) has also been tested in the OGDR experiment.

Figure 6 shows some oscilloscope traces of the OG signal modulated at ω_1. One notices a change in the signal polarity from positive to negative with increasing neon pressure. In Figs. 6(b)—6(d), some additional spikes are seen on the leading and/or trailing edges of the modulated wave forms. Spikes of this kind were observed whenever the OG signal was about to reverse its polarity due to a change in the discharge condition. This seems to indicate that the spikes observed in the OG signal are associated with competing time-dependent relaxation processes of the excited levels in the discharge, although the origin of the spikes has not yet been examined in any further detail. Under the discharge conditions where the modulated OG signals are accompanied by spikes of this kind, Eq. (51) has to be taken as a rough estimate for the determination of the polarity of S_D. In addition, it was important that the laser beams did not hit the cathode wall to get a valid phase relation given by Eq. (51).

C. OODR experiment

An OODR experiment was also carried out using the same experimental apparatus, allowing a direct comparison with the OGDR experiment. The experimental arrangement employed was in principle the same as that shown in Fig. 3, where only laser II was modulated at ω_2.

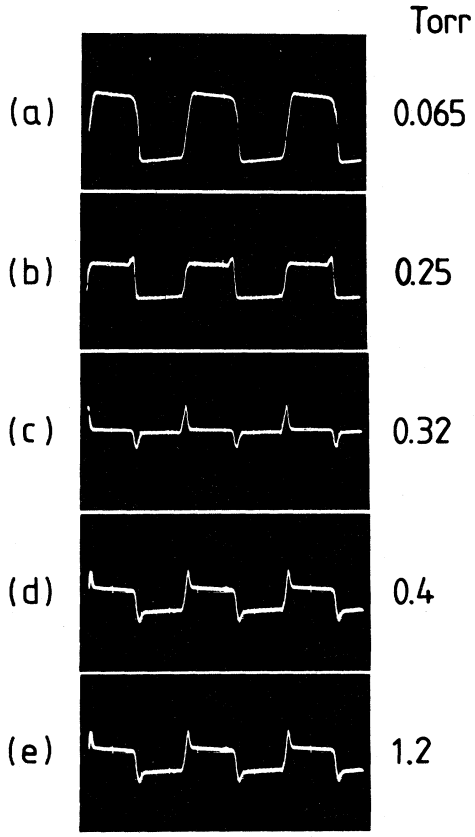

FIG. 6. Oscilloscope traces of the OG signal at ω_1 for the pump transition $1s_5$-$2p_4$. Discharge current is 12 mA, the power of laser I is 4 mW, and the time scale is 0.5 msec/division.

The transmitted intensity of the unmodulated laser I was greatly attenuated and detected with a photodiode placed far away from the discharge tube in order to suppress contributions due to the interfering radiation from the discharge plasma.[47] The absorption signal was analyzed at ω_2 with a lock-in amplifier, and the OODR signal S_0 was measured on a strip chart recorder.

IV. RESULTS

In the OGDR experiment, the modulated power of lasers I and II was restricted to less than 12 and 150 mW, respectively, in order to maintain the small signal limit. For these laser powers, the maximum single and double resonance signals observed were typically $S_I = 200$ mV and $S_D = 20$ mV. As expected, S_D was in all cases much smaller than S_I and S_{II}.

In Figs. 7—10 shown below the measured points are connected in all cases by lines. These lines are not theoretical curves, but they are simply given to guide the eye. By varying the pressure and current of the discharge the plasma parameters are changed. Since it is not the purpose of this paper to determine the individual rates which are responsible for the OG signal amplitude, the following measurements are primarily designed to demonstrate that the OGDR signal S_D is in general directly related to a linear combination of the single resonance amplitude, S_I and S_{II}.

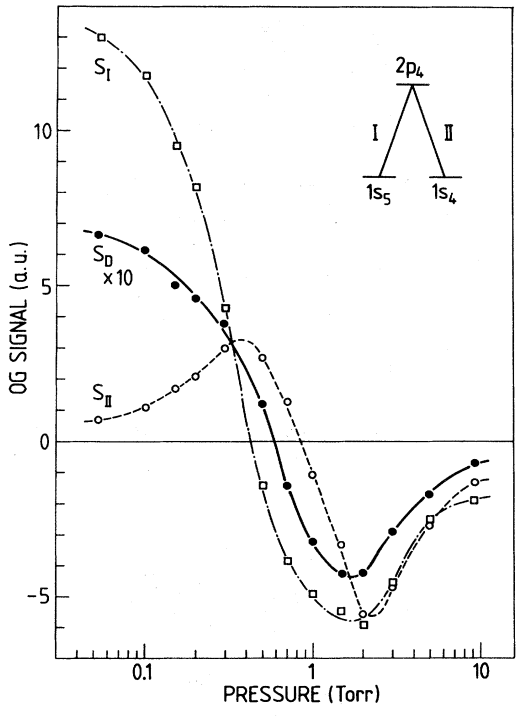

FIG. 7. Dependence of the OG signals on the neon pressure. Discharge current is 12 mA, and the powers of lasers I and II are 5 and 50 mW, respectively.

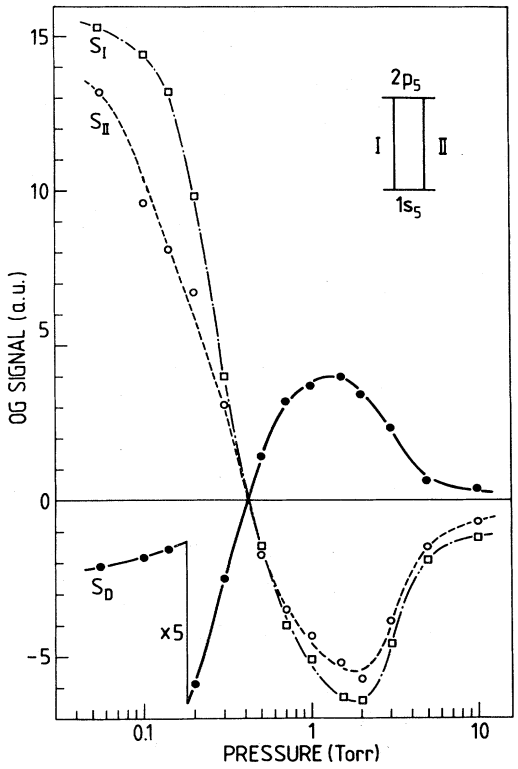

FIG. 8. Dependence of the OG signals on the neon pressure. Discharge current is 12 mA, and the powers of lasers I and II are 10 and 70 mW, respectively.

A. OG signal and polarity

Figure 7 shows the observed dependence of the OG signals S_I, S_{II}, and S_D on the neon pressure for a Λ-type double resonance, in which the transition employed for the measurement are indicated. With increasing neon pressure, the single-resonance signals S_I and S_{II} start with a positive polarity, decrease rapidly, and change their sign. Note the relation among the polarities of S_I, S_{II}, and S_D. In agreement with the theoretical prediction, case (a) in Table II, S_D is positive in the region of $S_I > 0$ and $S_{II} > 0$, and negative in the region of $S_I < 0$ and $S_{II} < 0$. In the pressure region of $S_I S_{II} < 0$ where S_D may be negative or positive, the amplitude of S_D is found to become small, even if the individual amplitudes S_I and/or S_{II} are fairly large. This result is due to the fact that two different OG functions in Eq. (48) or (49) contribute to S_D with opposite sign.

Figure 8 shows S_I, S_{II}, and S_D for a P-type double resonance measured as a function of the neon pressure. In contrast to the result shown in Fig. 7, a completely different situation is observed for the polarity of S_D: For $S_I > 0$ and $S_{II} > 0$, $S_D < 0$; for $S_I < 0$ and $S_{II} < 0$, $S_D > 0$, which also agrees with the theoretical prediction shown in Table II.

For a N-type double resonance, Fig. 9(a) shows the dependence of S_I, S_{II}, and S_D on the neon pressure, and

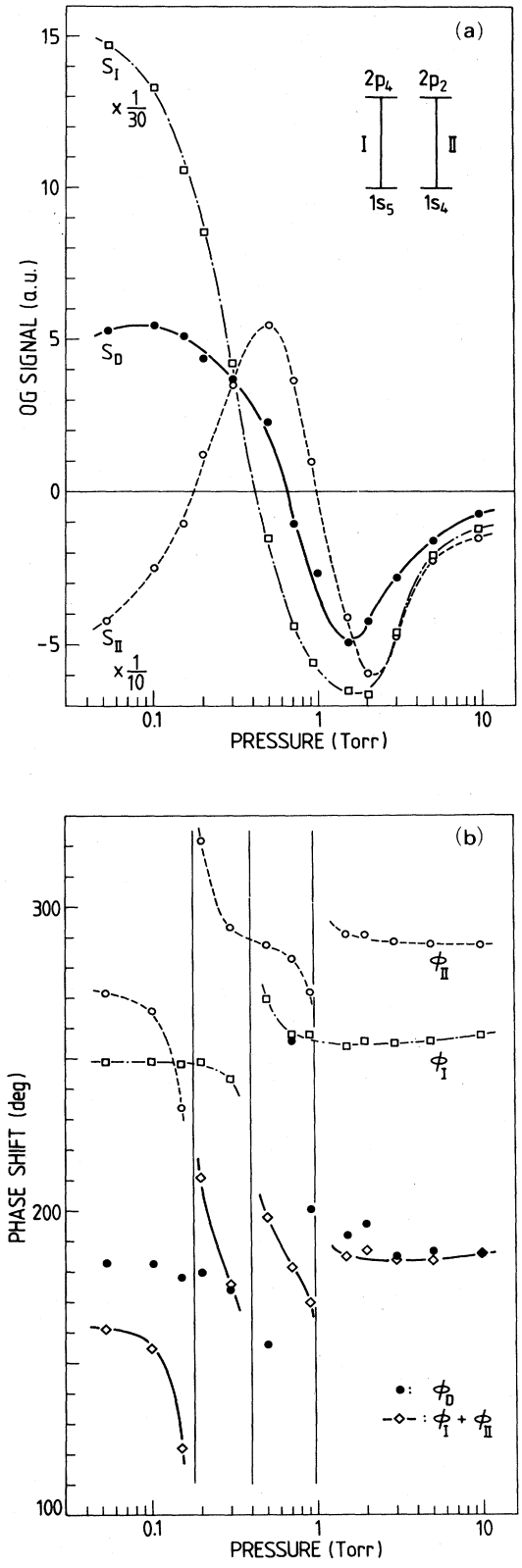

FIG. 9. Dependence of the OG signals (a) and the phase angles (b) on the neon pressure. Discharge current is 12 mA, and the powers of lasers I and II are 5 and 60 mW, respectively.

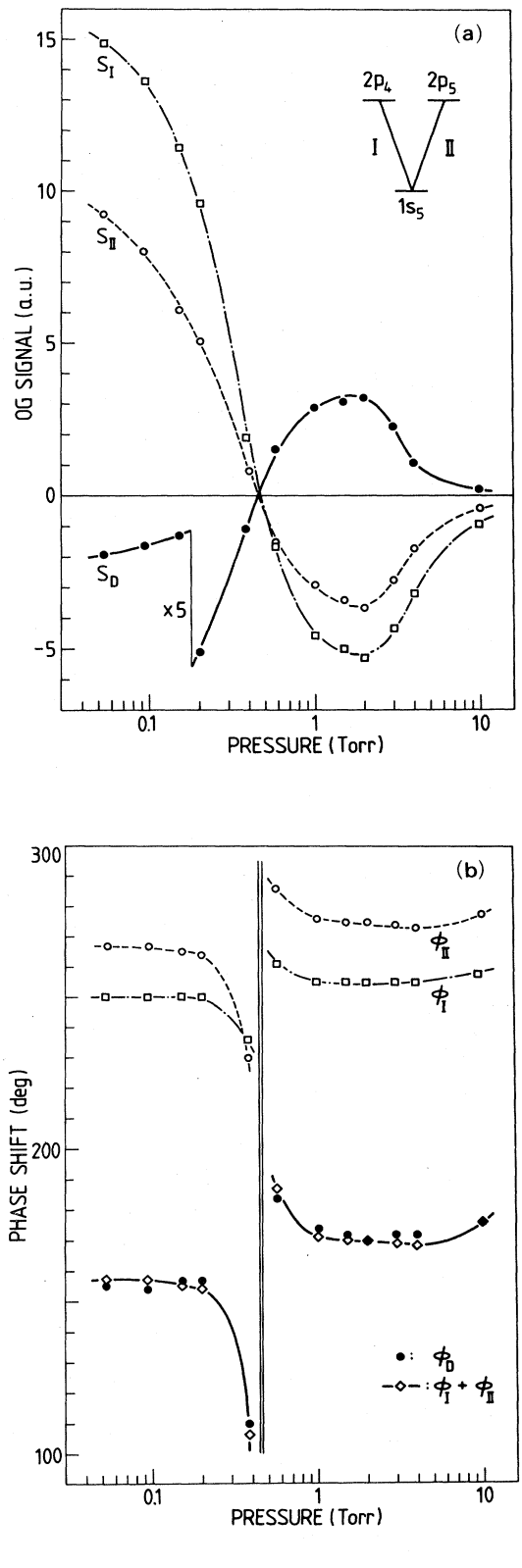

FIG. 10. Dependence of the OG signals (a) and the phase angles (b) on the neon pressure. Discharge current is 12 mA, and the powers of lasers I and II are 3 and 90 mW, respectively.

Fig. 9(b) shows the result of the simultaneous measurement of the phase angles ϕ_I, ϕ_{II}, and ϕ_D. With respect to the OG signal polarity, results are obtained which are in agreement with the theoretical predictions and are similar to those in case of the Λ-type double resonance. On the other hand, ϕ_I, ϕ_{II}, and ϕ_D are found to nearly follow the phase relation given by Eq. (51). When one of the OG signals S_I and S_{II} tends to be fairly small and to change its sign with increasing or decreasing neon pressure, one notices a slight departure from the phase relation expected. As mentioned in Sec. III B, this deviation from the ideal phase relation is due to the spikes which appear in the modulated OG signals. However, it is clear that Eq. (51) still provides a useful relation to determine the absolute polarity of S_D even under such discharge conditions.

For a V-type double resonance, Figs. 10(a) and 10(b) show the OG signals and the phase angles measured as a function of the neon pressure. The polarities of S_I, S_{II}, and S_D are found to change according to the theoretical prediction, which are similar to those for the P-type double resonance shown in Fig. 8. The phase relation expected is clearly demonstrated in Fig. 10(b) over the whole range of the neon pressure.

Under the discharge condition providing $S_I S_{II} > 0$, the OG signals S_I, S_{II}, and S_D have also been measured as a function of the laser power and as a function of the discharge current. The polarity of OG signals was never found to be affected by the laser power, as expected from Eqs. (46), (47), and (49). Also, the theoretical prediction on the signal polarity has been confirmed over the range of the laser power and the discharge current investigated.

The experimental results on the polarity of the OG signals show that in the neon discharge employed, radiative processes dominate the relaxation of the excited levels concerned. Otherwise, S_D should appear with an identical polarity for all four types of double resonances, as shown in case (b) and (c) of Table II. On the other hand, the definite phase relations observed for ϕ_I, ϕ_{II}, and ϕ_D suggest that the basic assumption of a fast relaxation of the modulated population densities is very reasonable.

B. OGDR and OODR spectra

As shown in previous sections, the OGDR signal S_D for the neon plasma has an identical polarity for the V- and P-type double resonances, which is opposite to that for the N- and Λ-type double resonances. If an OGDR spectrum is observed under discharge conditions providing $S_I S_{II} > 0$, the polarity of the individual spectral lines immediately allows one to extract those transitions which have a common lower level with the pump transition, as mentioned in Sec. II. The OODR technique provides basically a state-selective spectrum similar to the OGDR spectrum. The state-selective OGDR and OODR spectra have been observed by tuning the output frequency of laser I to a specific resonant transition and by scanning laser II over its entire possible tuning range.

Some examples of the OGDR and OODR spectra are shown in Fig. 11 where the metastable $1s_5$ level has been pumped by laser I. The spectral lines which have the same negative polarity in the OG single-resonance spectrum [Fig. 11(a)], are found to be divided into two groups in the OGDR spectrum [Fig. 11(b)]: Those spectral lines which share the common lower $1s_5$ level are observed with a positive sign, whereas the other lines originating from a N- or Λ-type double resonance appear with a negative sign. The same state selectivity can also be observed in the OODR spectrum [Fig. 11(c)]. However, a few spectral lines are found to be missing in Fig. 11(c), and the signal-to-noise ratio (S/N) in Fig. 11(b) is much better than that in Fig. 11(c). Although the S/N ratio in the OODR spectrum has been improved by changing the discharge condition [Fig. 11(d)], some of the spectral lines are still very weak.

In Fig. 12, other examples of double-resonance spectra are presented which have been obtained by pumping the nonmetastable $1s_4$ level. With respect to the state selectivity and the S/N ratio, the OGDR and OODR spectra show the characteristic features very similar to the spectra shown in Fig. 11.

In contrast to the other transitions, the transition $1s_2$-$2p_1$ shows a positive sign in the OGDR spectra [Figs. 11(b) and 12(b)], although this transition originates from a N-type double resonance. This is due to the fact that the discharge condition necessary to the state selectivity, i.e., $S_I S_{II} > 0$, is not satisfied for this transition, as seen in the OG single-resonance spectrum [Fig. 11(a) or 12(a)]. The constraint of the discharge condition is removed in the OODR experiment, and a uniform signal polarity is achieved as shown in Figs. 12(c) and 12(d).

V. DISCUSSION

The OGDR technique has been demonstrated to provide a state-selective spectroscopic method for studying transitions between excited levels in a plasma. One of the most significant applications of this technique is, therefore, the spectral analysis of atomic and molecular transitions embedded in dense and complex spectra which may be created in discharges, flames, and other plasma sources. The spectra usually observed contain a lot of components originating from different atomic and/or molecular species. As discussed in Sec. II, the OGDR experiment in such plasmas is able to provide simple double-resonance spectra, depending on the dominant relaxation processes of the perturbed population densities in the plasma. In addition to the OGDR spectra presented in the preceding section, we have recently observed very simple OGDR spectra in molecular hydrogen and nitrogen discharges, where state selectivity and signal polarity are in good agreement with the theoretical predictions.[48] Those experiments correspond to the plasma model of case (b) or (c) discussed in Sec. II D.

As described in Sec. II and demonstrated in Sec. IV, the conventional OODR technique is another useful method for state-selective spectroscopy in plasmas. However, the OODR technique has some disadvantages. For the sensitive detection of small absorptions, a narrow-band probe laser has to be employed, and a rather long plasma column is often required for the OODR experiment. Moreover, the sensitivity of the OODR is limited by spontaneous emission from the plasma, the fluctuations of the

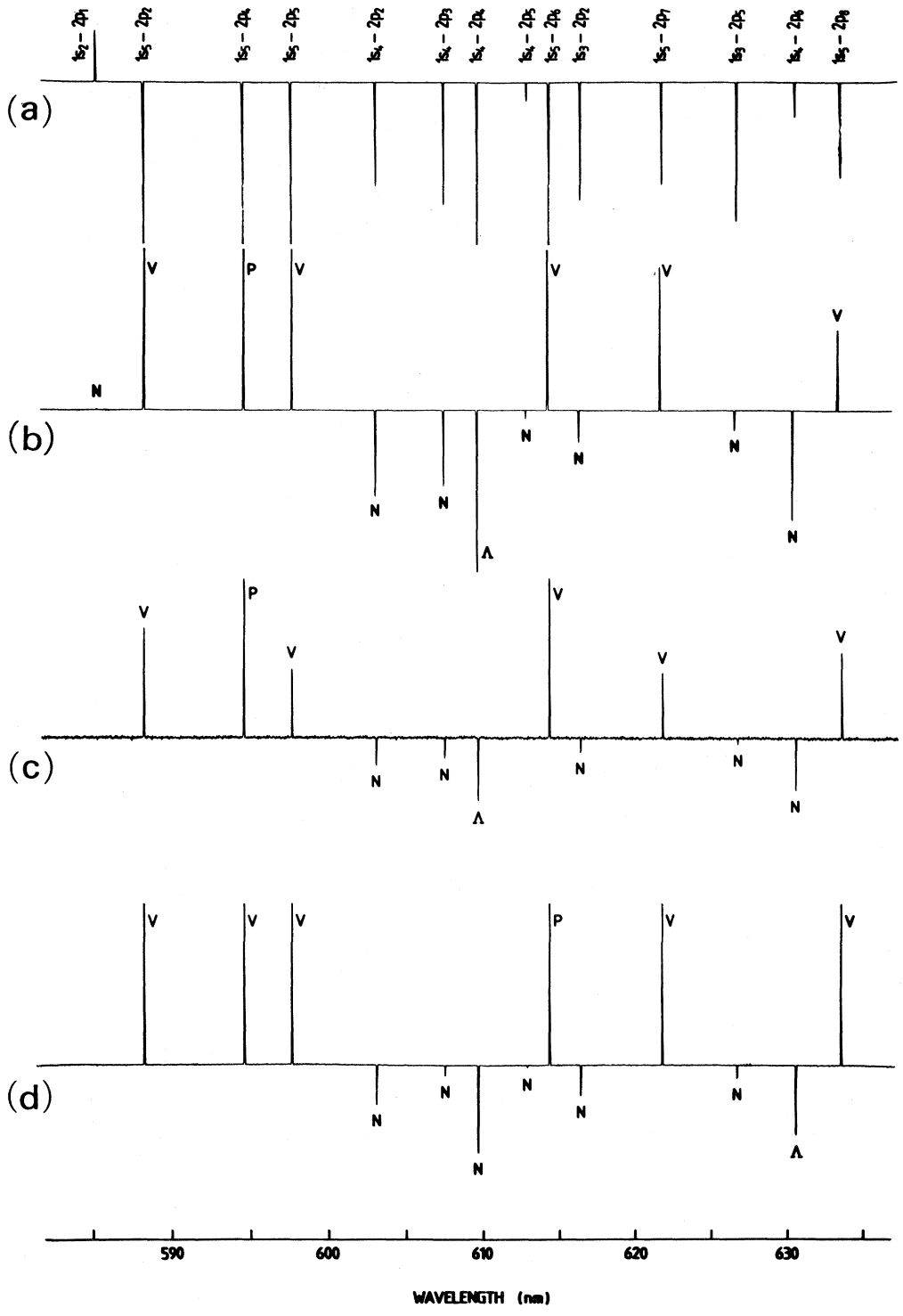

FIG. 11. Double-resonance spectra in neon observed by pumping the $1s_5$ level with laser I. (a) OG single-resonance spectrum taken for reference at a neon pressure of 2.0 Torr, a discharge current of 4 mA, and a maximum power of laser II of 120 mW; (b) OGDR spectrum taken at a neon pressure of 2.0 Torr, a discharge current of 4 mA, a power of laser I of 6 mW, and a maximum power of laser II of 100 mW; (c) OODR spectrum taken at a neon pressure of 1.5 Torr, a discharge current of 4 mA, a power of laser I of 6 mW, and a maximum power of laser II of 170 mW; (d) OODR spectrum taken at a neon pressure of 0.08 Torr, a discharge current of 12 mA, a power of laser I of 3 mW, and a maximum power of laser II of 150 mW. Time constant of the lock-in amplifier is 125 msec, and the scan rate is about 34 Å/min.

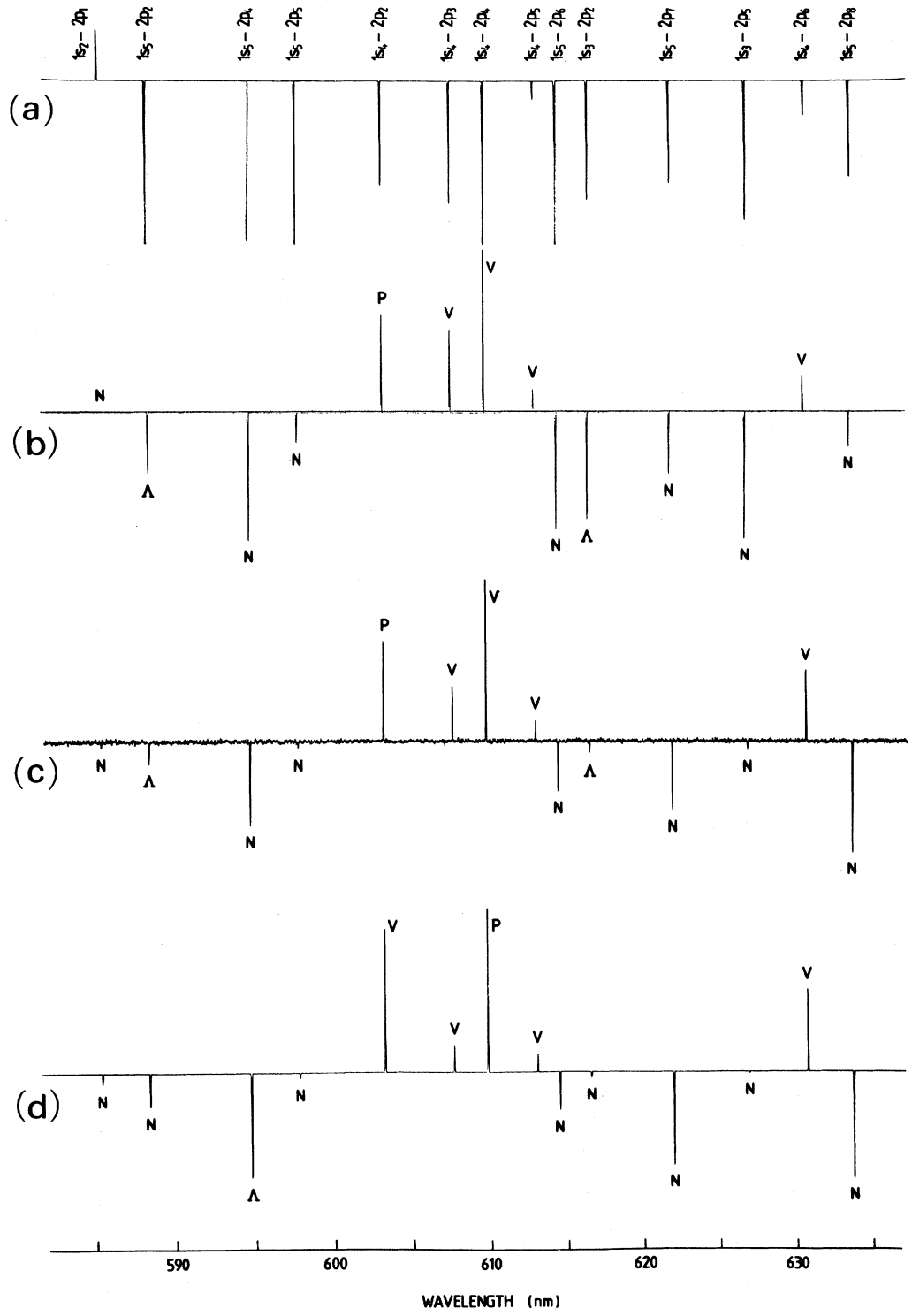

FIG. 12. Double-resonance spectra in neon observed by pumping the $1s_4$ level with laser I. (a) Same reference spectrum as in Fig. 11(a); (b) OGDR spectrum taken at a power of laser I of 11 mW and a maximum power of laser II of 140 mW; (c) OODR spectrum taken at a power of laser I of 5 mW and a maximum power of laser II of 170 mW; (d) OODR spectrum taken at a power of laser I of 3 mW and a maximum power of laser II of 150 mW. Other experimental conditions for each spectrum are the same as in Fig. 11.

laser power, and the detector noise. On the other hand, the OGDR technique is essentially unaffected by the plasma radiation. The laser spectrum should only be narrower than the separation between adjacent spectral lines of interest. The OG signal observed is rather insensitive to the laser noise. Furthermore, both pump transitions are able to enhance the OGDR signal amplitude, as seen from Eq. (48) or (49), whereas only a single transition is responsible for the OODR signal amplitude.

The OGDR technique is expected to open up new possibilities for the quantitative analysis of atomic and molecular processes in plasmas. For example, from Eqs. (46) and (48) for the P-type double resonance, one obtains an approximate relation

$$S_D/S_I \approx -P_{20}\tau_1 = -I_{20}\sigma_{12}\tau_1 \ . \tag{52}$$

When σ_{12} is known, Eq. (52) may be used for the determination of the effective lifetime τ_1 of level $|1\rangle$ in the discharge, which is given by a measurement of S_D/S_I as a function of I_{20}. Similar approximate relations may be derived for studies of specific collisional energy-transfer processes in N-type double resonances.

As a further application, the Doppler-free technique[2–8] can be introduced in the OGDR experiment to get a high resolution, state-selective spectrum. The extension of the present theory to the Doppler-free case can be done by incorporating the Doppler effect and the spectral line shape in P_1 and P_2.[45]

Finally, we want to mention other types of double resonance than those discussed so far. When atoms or molecules in the ground state are pumped or intense laser beams are employed in the experiment, one may observe the OGDR signal arising from the stepwise excitation by two laser photons such as three-level double resonances where a common intermediate level is present, and four-level double resonances with two independent intermediate levels. The present theory can, of course, be applied to these cases, if an appropriate interaction matrix $\underline{F}$ is determined to get the analytical expression for S_D. It is clear that the OGDR experiment described in this paper is different in nature from the previous OG experiments[11–14] using two cw or pulsed dye lasers in which two-step one-photon excitations have been observed in atomic discharges.

VI. CONCLUSION

The new OGDR spectroscopy has been studied theoretically and experimentally. A general formalism has been developed for the analysis of the double-resonance experiments. It has been applied to derive analytical expressions for the OG single- and double-resonance signals, as well as the conventional OODR signal for comparison. The results predict that the OGDR signal polarity is characteristic to the N-, Λ-, V-, and P-type double resonances and suggest that the OGDR technique allows one to observe state-selective spectra in a plasma. The characteristic OGDR signal polarities have been confirmed by experiments using a homemade hollow-cathode discharge in neon and two commercial cw dye lasers. State-selective spectra in the neon discharge are shown, together with OODR spectra. The discussion has shown possible applications of the OGDR technique, especially, to the state-selective spectroscopy of excited atoms and molecules in a discharge, and the advantages with respect to the conventional OODR technique are pointed out.

ACKNOWLEDGMENTS

The authors thank P. Klopotek for helpful discussions and B. Steffes, M. Kittl, and J. Füllsack for their excellent technical assistance. One of the authors (K.M.) is grateful to the Max-Planck Institut for providing him a Visiting Fellowship and to the Electrotechnical Laboratory for support.

APPENDIX

Here we discuss the OGDR signal for the case (a) described in Sec. II D. In this case, S_D for the N-type double resonance is calculated from Eq. (49) as

$$S_D = \tfrac{1}{2}\eta P_{10}P_{20}[(N_1^0 - N_2^0)\tau_3(A_{23}\tau_2)g(3,4) + (N_3^0 - N_4^0)\tau_1(A_{41}\tau_4)g(1,2)]/[f_3(1,2;3,4)]_0 \ , \tag{A1}$$

where $g(i,j)$ and $f_m(i,j;k,l)$ are the functions $G(i,j)$ and $F_m(i,j;k,l)$ for $u_{13}=u_{24}=1$, $C_{ik}=C_{jl}=0$, $\Phi_{ji}=A_{ji}$, $\Phi_{jk}=A_{jk}$, and $\Phi_{lk}=A_{lk}$. For the discharge condition providing $S_I S_{II} > 0$ or $g(1,2)g(3,4) > 0$, Eq. (A1) indicates that S_D has the same polarity as S_I and S_{II}. Furthermore, if $A_{23} \approx 0$ and $A_{41} \approx 0$, no OGDR signal of this type exists.

Equation (49) for the Λ-type double resonance reduces to

$$S_D = \tfrac{1}{2}\eta P_{10}P_{20}\tau_2[(N_1^0 - N_2^0)(A_{23}\tau_3 - 1)g(3,2) + (N_3^0 - N_2^0)(A_{21}\tau_1 - 1)g(1,2)]/[f_3(1,2;3,2)]_0 \ . \tag{A2}$$

In a weakly ionized plasma of interest where one can reasonably assume $N_2^0 \ll N_1^0$ and $N_2^0 \ll N_3^0$, the effective lifetimes τ_1 and τ_3 of the lower levels are expected to be very much longer than the radiative lifetimes A_{21}^{-1} and A_{23}^{-1} of the upper level $|2\rangle$, i.e., $A_{21}\tau_1, A_{23}\tau_3 \gg 1$. Therefore, for $S_I S_{II} > 0$, S_D given by Eq. (A2) is expected to have the same polarity as S_I and S_{II}. This polarity relation can be shown to be unaffected by strong collisional interactions between the upper levels.

The function $h(1,2;1,4)$ and $h(1,4;1,2)$ for the V-type double resonance and the function $h(1,2;1,2)$ for the P-type double resonance are found to be always negative taking into account the fact that $\Phi_{21}\tau_2, \Phi_{41}\tau_4 < u_{24} \approx 1$ for typical discharge conditions of interest. Hence if a plasma is generated with $S_I S_{II} > 0$, S_D for the V- and P-type double resonances should have a polarity opposite to that of S_I and/or S_{II}. This can be seen more clearly from the simplified expressions for S_D: For the V-type double resonance,

$$S_D = -\tfrac{1}{2}\eta P_{10}P_{20}\tau_1[(N_1^0-N_2^0)(1-A_{21}\tau_2)g(1,4)+(N_1^0-N_4^0)(1-A_{41}\tau_4)g(1,2)]/[f_3(1,2;1,4)]_0 , \quad \text{(A3)}$$

and for the P-type double resonance,

$$S_D = -\eta P_{10}P_{20}(N_1^0-N_2^0)[\tau_1(1-A_{21}\tau_2)+\tau_2]g(1,2)/[f_3(1,2;1,2)]_0 . \quad \text{(A4)}$$

---

*Permanent address: Electrotechnical Laboratory, 1-1-4 Umezono, Sakura-mura, Niihari-gun, Ibaraki 305, Japan.

[1]For a review, see, e.g., J. E. M. Goldsmith and J. E. Lawler, Contemp. Phys. 22, 235 (1981).
[2]J. E. Lawler, A. I. Ferguson, J. E. M. Goldsmith, D. J. Jackson, and A. L. Schawlow, Phys. Rev. Lett. 42, 1046 (1979).
[3]D. J. Jackson, H. Gerhardt, and T. W. Hänsch, Opt. Commun. 37, 23 (1981).
[4]D. R. Lyons, A. L. Schawlow, and G.-Y. Yan, Opt. Commun. 38, 35 (1981).
[5]C.-J. Lorenzen and K. Niemax, Opt. Commun. 43, 26 (1982).
[6]T. Suzuki and M. Kakimoto, J. Mol. Spectrosc. 93, 423 (1982).
[7]J. E. M. Goldsmith, A. I. Ferguson, J. E. Lawler, and A. L. Schawlow, Opt. Lett. 4, 230 (1979).
[8]J. E. M. Goldsmith and A. V. Smith, Opt. Commun. 32, 403 (1982).
[9]J. E. M. Goldsmith, Opt. Lett. 7, 437 (1982).
[10]G. C. Bjorklund, R. R. Freeman, and R. H. Storz, Opt. Commun. 31, 47 (1979).
[11]R. Engleman, Jr. and R. Keller, Opt. Lett. 5, 465 (1980).
[12]R. Shuker, A. Ben-Amar, and G. Erez, Opt. Commun. 39, 51 (1981).
[13]C. Delsart, J.-C. Keller, and C. Thomas, J. Phys. B 14, 3355 (1981).
[14]P. Camus, M. Dieulin, and A. El Himdy, Phys. Rev. A 26, 379 (1982).
[15]P. Hannaford and G. W. Series, Phys. Rev. Lett. 48, 1326 (1982); J. Phys. B 14, L661 (1981).
[16]A. Ben-Amar, R. Shuker, and G. Erez, Appl. Phys. Lett. 38, 763 (1981).
[17]C. P. Ausschnitt, G. C. Bjorklund, and R. R. Freeman, Appl. Phys. Lett. 33, 851 (1978).
[18]G. C. Bjorklund, C. P. Ausschnitt, R. R. Freeman, and R. H. Storz, Appl. Phys. Lett. 33, 54 (1978).
[19]T. F. Johnston Jr., Laser Focus 14, 58 (1978).
[20]R. B. Green, R. A. Keller, G. G. Luther, P. K. Schenk, and J. C. Travis, IEEE J. Quantum Electron. QE-13, 63 (1977).
[21]M. J. Kavaya, R. T. Menzies, and U. P. Oppenheim, IEEE J. Quantum Electron. QE-18, 19 (1982).
[22]S. Moffatt and A. L. S. Smith, Opt. Commun. 37, 119 (1981).
[23]R. B. Green, R. A. Keller, G. G. Luther, P. K. Schenck, and J. C. Travis, Appl. Phys. Lett. 29, 727 (1976).
[24]W. B. Bridges, J. Opt. Soc. Am. 68, 352 (1978).
[25]R. A. Keller and E. F. Zalewski, Appl. Opt. 19, 3301 (1980).
[26]P. K. Schenck, W. G. Mallard, J. C. Travis, and K. C. Smyth, J. Chem. Phys. 69, 5147 (1978).
[27]D. Feldmann, Opt. Commun. 29, 67 (1979).
[28]C. Demuynck and J. L. Destombes, IEEE J. Quantum Electron. QE-17, 575 (1981).
[29]D. M. Pepper, IEEE J. Quantum Electron. QE-14, 971 (1978).
[30]K. Smith and P. K. Schenck, Chem. Phys. Lett. 55, 466 (1978).
[31]G. Erez, S. Lavi, and E. Miron, IEEE J. Quantum Electron. QE-15, 1328 (1979).
[32]E. F. Zalewski, R. A. Keller, and R. Engleman, Jr., J. Chem. Phys. 70, 1015 (1979).
[33]J. E. Lawler, Phys. Rev. A 22, 1025 (1980).
[34]C. Drèze, Y. Demers, and J. M. Gagné, J. Opt. Soc. Am. 72, 912 (1982).
[35]W. J. van den Hoek and J. A. Visser, J. Appl. Phys. 51, 5292 (1980).
[36]I. M. Beterov and N. V. Fateyev, Opt. Commun. 40, 425 (1982).
[37]R. Shuker, A. Ben-Amar, and G. Erez, Opt. Commun. 42, 29 (1982).
[38]C. R. Vidal, Opt. Lett. 5, 158 (1980).
[39]W. Demtröder, Phys. Rep. 7C, 223 (1973).
[40]C. Wieman and T. W. Hänsch, Phys. Rev. Lett. 36, 1170 (1976).
[41]Note that no details of the modulation-wave form have to be specified.
[42]The modulation depths of the frequency components of $\vec{n}$ at ω_1, ω_2, and ω_D are given by $2\vec{n}^{\,I}$, $2\vec{n}^{\,II}$, and $\vec{n}^{\,D}$, respectively.
[43]R. G. Gordon and J. I. Steinfeld, in *Molecular Energy Transfer,* edited by R. D. Levine and J. Jortner (Israel University Press, Jerusalem, 1976), p. 67.
[44]J. I. Steinfeld and P. L. Houston, in *Lasers and Coherence Spectroscopy,* edited by J. I. Steinfeld (Plenum, New York, 1978), p. 1.
[45]K. Shimoda, in *Laser Spectroscopy of Atoms and Molecules,* edited by H. Walther (Springer, Berlin, 1976), p. 197.
[46]S. Inatsugu and J. R. Holmes, Phys. Rev. A 11, 26 (1975).
[47]The calculated full width at half maximum of a neon spectrum at room temperature is about 2.6 GHz and is comparable to the spectral width of laser I. Therefore, no spectral narrowing of laser I has been made for the OODR experiment.
[48]K. Miyazaki, H. Scheingraber, and C. R. Vidal, Phys. Rev. Lett. 50, 1046 (1983).